GEOPHYSICS, VOL. 63, NO. 1 (JANUARY-FEBRUARY 1998); P. 109–119, 14 FIGS.

3-D inversion of gravity data

Yaoguo Li* and Douglas W. Oldenburg*

ABSTRACT

We present two methods for inverting surface gravity data to recover a 3-D distribution of density contrast. In the first method, we transform the gravity data into pseudomagnetic data via Poisson's relation and carry out the inversion using a 3-D magnetic inversion algorithm. In the second, we invert the gravity data directly to recover a minimum structure model. In both approaches, the earth is modeled by using a large number of rectangular cells of constant density, and the final density distribution is obtained by minimizing a model objective function subject to fitting the observed data. The model objective function has the flexibility to incorporate prior information and thus the constructed model not only fits the data but also agrees with additional geophysical and geological constraints. We apply a depth weighting in the objective function to counteract the natural decay of the kernels so that the inversion yields depth information. Applications of the algorithms to synthetic and field data produce density models representative of true structures. Our results have shown that the inversion of gravity data with a properly designed objective function can yield geologically meaningful information.

INTRODUCTION

Gravity surveys have been used in investigations of wide range of scales such as tectonic studies and mineral explorations (Paterson and Reeves, 1985) and in engineering and environmental problems (Hinze, 1990; Ward, 1990). The inversion of gravity data constitutes an important step in the quantitative interpretation since construction of density contrast models markedly increases the amount of information that can be extracted from the gravity data. However, a principal difficulty with the inversion of gravity data is the inherent nonuniqueness that exists in any geophysical method based upon a static potential field. Since the gravity field is known only on the surface of the earth, there are infinitely many equivalent density distributions beneath the surface that will reproduce the known field. One such distribution is an infinitesimally thin layer of mass just beneath the surface. This means that there is no inherent depth resolution associated with the gravity data. In addition, there is also nonuniqueness that arises from the availability of only a finite number of inaccurate measurements. If there is one model that fits the data, there will be infinitely many models that fit the data to the same degree.

To overcome this difficulty, other authors have used several approaches to introduce prior information into the inversion so that a unique solution is obtained. Some authors prescribe the density variation and seek to invert for the geometrical parameters of the model. The most noticeable application is the inversion for the thickness of sedimentary basin given the density variation as a function of depth (e.g., Oldenburg, 1974; Pedersen, 1977; Chai and Hinze, 1988; Reamer and Ferguson, 1989; Guspi, 1990). Alternatively, others assume a constant density contrast and invert for the position of a polygonal (in 2-D) or polyhedral (in 3-D) body from isolated anomalies (e.g., Pedersen, 1979). In an effort to introduce more qualitative prior information, some authors indirectly assume the shape or the center of the causative region and seek to construct a density contrast as a function of spatial position. This approach has been used most often in inversions to recover compact bodies with density contrasts. For example, Green (1975) guides the inversion by varying the reference model and associated weights constructed from available information, Last and Kubik (1983) minimize the total volume of the causative body, and Guillen and Menichetti (1984) minimize the inertia of the body with respect to the center of the body or an axis passing through it. These are rather specific forms of prior information and some are only suited for recovering a single body.

For more complicated situations, the inversion must be capable of incorporating different types of prior knowledge and user-imposed constraints so that realistic density models can be constructed that not only fit the data but also agree with other available constraints on the earth model. Our algorithm is analogous to the 3-D magnetic inversion algorithm of Li and Oldenburg (1996) and the reader is referred to that paper for

Presented at the 65th Annual International Meeting, Society of Exploration Geophysicists. Manuscript received by the Editor April 26, 1996; revised manuscript received April 4, 1997.
*Dept. of Earth and Ocean Sciences, UBC-Geophysical Inversion Facility, University of British Columbia, 2219 Main Mall, Vancouver, B.C. V6T 1Z4, Canada. E-mail: li@geop.ubc.ca;doug@geop.ubc.ca.

details. Basically, we first divide the earth into rectangular cells of constant but unknown density. The densities are found by minimizing a model objective function subject to fitting the observed data. The objective function includes terms that penalize discrepancies from a reference model and also roughness in different spatial directions. It incorporates a depth weighting function designed to distribute the density with depth and it also has additional 3-D weighting functions to incorporate further information about the density that might be available from other geophysical surveys, geological data, or the interpreter's understanding of the local geology. These 3-D weighting functions can also be used to explore the nonuniqueness of the inversion, or to carry out hypothesis testing that might answer questions about the presence of features recovered in previous inversions. Finally, positivity can be imposed to obtain a nonnegative density distribution. The minimization of an objective function subject to fitting the data is achieved by using a generalized subspace inversion algorithm. This avoids the computational difficulties associated with the solution of large matrix systems.

The availability of a 3-D magnetic inversion algorithm allows an alternative route for inverting gravity data. Using Poisson's relation between gravity and magnetic fields, gravity data can in theory be inverted after transforming the gravity data into pseudomagnetic data that would have been observed under a user-specified inducing field direction. This is a viable approach if the transformation can be carried out. In this paper, we first present the inversion of gravity data by using a magnetic inversion algorithm based upon Poisson's relation and then develop the methodology for the direct gravity inversion. We illustrate the algorithms with both synthetic and field examples.

GRAVITY INVERSION USING A MAGNETIC INVERSION ALGORITHM

Gravity and magnetic fields produced by the same causative body are related to each other by Poisson's relation. Given a 2-D map of gravity data, one can generate corresponding pseudomagnetic data under any assumed directions of magnetization and anomaly projection. Thus, in theory, gravity data can be inverted indirectly by using a magnetic inversion algorithm.

Let $\mathbf{B}(\mathbf{r})$ be the magnetic field and $\mathbf{F}(\mathbf{r})$ be the gravity field produced by a causative body that has susceptibility κ and a density ρ. If κ and ρ have a constant ratio, Poisson's relation states that (e.g., Grant and West, 1965), in the case of induced magnetization, the magnetic field $\mathbf{B}$ and gravity field $\mathbf{F}$ satisfy the relation,

$$\mathbf{B}(\mathbf{r}) = \frac{B_0 \kappa}{4\pi\gamma\rho} \frac{\partial}{\partial \hat{u}} \mathbf{F}(\mathbf{r}), \tag{1}$$

where B_0 is the strength of the inducing magnetic field in the direction of $\hat{u}$, γ is the gravitational constant, and $\partial/\partial\hat{u}$ denotes the directional derivative. Based on this relation, it can be shown that the magnetic data $B_v(x, y)$ (the projection of $\mathbf{B}$ in the direction $\hat{v}$) are related to the gravity data $F_z(x, y)$ (the vertical component of $\mathbf{F}$) by the following equation in the wavenumber domain (see Appendix for derivation and numerical considerations),

$$\tilde{B}_v(p, q) = \frac{B_0 \kappa}{4\pi\gamma\rho} \tilde{F}_z(p, q) \frac{(\hat{u} \cdot \mathbf{K})(\hat{v} \cdot \mathbf{K})}{\sqrt{p^2 + q^2}}. \tag{2}$$

In equation (2) $\tilde{B}_v(p, q)$ is the Fourier transform of the magnetic data $B_v(x, y)$, $\tilde{F}_z(p, q)$ is the Fourier transform of the gravity data, (p, q) are the wavenumbers in the x- and y-directions, and $\mathbf{K} = (ip, iq, \sqrt{p^2 + q^2})$ with $i = \sqrt{-1}$. The operator in equation (2) is the inverse of that used in the calculation of pseudogravity data from magnetic data (Baranov, 1957; Bhattacharyya, 1965) and it is stable at any magnetic latitude when the gravity data are band limited. Equation (2) can be applied efficiently using the fast Fourier transform (FFT) when gridded data maps are available.

A suitable pseudomagnetic data set can thus be computed if we have gravity data, an assumed inducing magnetic field $\mathbf{B}_0 = B_0\hat{u}$, a specified direction $\hat{v}$ for the magnetic anomaly, and a constant ratio of susceptibility κ over the unknown density ρ. We can invert the pseudomagnetic data to recover a susceptibility model and then recover the density model using the assumed ratio of κ/ρ. For practical applications, it is convenient to choose $\kappa = 4\pi\gamma\rho$. Once the inversion of the pseudomagnetic data is completed, the density model ρ_c is obtained from the constructed susceptibility model κ_c by

$$\rho_c(\mathbf{r}) = \frac{\kappa_c(\mathbf{r})}{4\pi\gamma}. \tag{3}$$

Since the transformation to pseudomagnetic data is stable, this algorithm can work at any magnetic latitude. However, as the following discussion shows, the best inversion result is generally obtained by using an intermediate inclination. The transformation to pseudomagnetic data yields a map with zero dc component. This is the correct theoretical value when the map area approaches infinity but for finite areas encountered in practice, the dc component is generally nonzero. Thus, the mean value of the pseudomagnetic data is incorrect. The discrepancy decreases with magnetic latitude, so this problem can be alleviated partially by working at a lower latitude or near the equator. On the other hand, the pseudomagnetic anomaly is the most concentrated at the pole, but it spreads over a wide area that can extend beyond the original area of gravity data when the inclination approaches zero. In addition, linear structures aligned with declination of the inducing field have small magnetic responses at low latitude. These considerations suggest the use of a high latitude. Thus an intermediate latitude provides a trade off between two extremes. Numerical tests have shown that the best density model is obtained when working at a middle latitude and the solution degrades when the latitude approaches either 0° or 90°. For this reason, we prefer to work at intermediate latitudes and choose a declination sufficiently different from the strike direction of the dominant linear trends in the data.

Figure 1 displays one cross-section and two plan-sections of a density model that consists of a dipping dyke with a density contrast of 1.0 g/cm^3 embedded in a uniform half-space. Figure 2 is the surface gravity anomaly produced by the model in Figure 1. The map consists of 441 data and each datum has been contaminated with Gaussian noise whose standard deviation is equal to 2% of the accurate datum magnitude. Figure 3 displays the total field pseudomagnetic anomaly derived from the noise-contaminated gravity data in Figure 2. The inducing field has an assumed strength of $B_0 = 50000$ nT and a direction of $I = 45^\circ$ and $D = 45^\circ$. A low-pass filter has been applied to the gravity data to suppress the effect of added noise (see Appendix).

The calculated pseudomagnetic data are then inverted to recover a susceptibility model using the algorithm of Li and Oldenburg (1996). The model consists of 4000 cubic cells (20 in each horizontal direction and 10 in the vertical) of 50 m on a side. Since the pseudomagnetic data are obtained by filtering noisy data, it is difficult to estimate the actual noise level for each resulting datum. The desired data misfit level is therefore unknown. For the current example, we assume a constant standard deviation for the noise associated with the pseudomagnetic data since they are linear functions of the initial gravity data with Gaussian noise. The target misfit is taken to be slightly higher than the lowest misfit value that is achievable. This model is converted to density by equation (3) and is shown in Figure 4. The dipping tabular shape is evident and the depth to the top of the high density region is close to the true value, although the recovered amplitude is about 35% higher than the true value. Over all, however, the constructed density model is a reasonable representation of the true structure.

The advantage of this approach is that only one inversion program is needed to perform the task of both gravity and magnetic inversion. The drawbacks are related mainly to the data transformation. First, equation (2) yields a magnetic map with zero dc component, and it is an incorrect mean value for finite areas of practical data sets. This will cause difficulties for the corresponding magnetic inversion. Second, and perhaps more important, the errors associated with the calculated pseudomagnetic data are unknown. It is then difficult to determine the appropriate level of data misfit. As a consequence, it becomes difficult to judge whether a particular structure in the recovered model is genuine or a result of over-fitting the data. Despite these practical difficulties in implementation, we have demonstrated that the indirect inversion of gravity data using

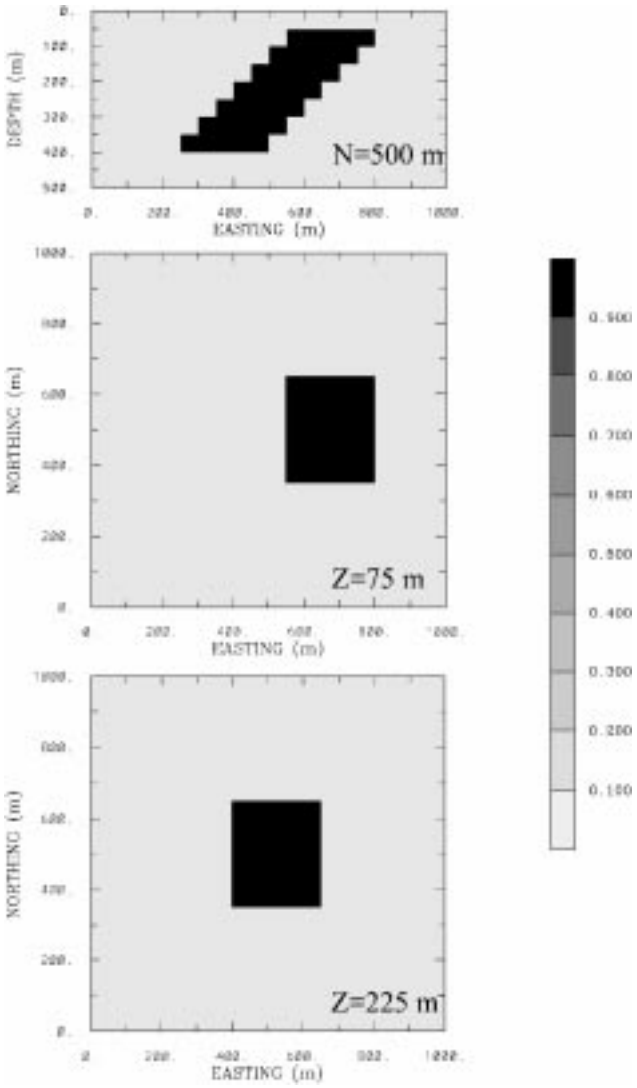

FIG. 1. Slices through a 3-D density model composed of a dipping dyke in a uniform background. The dyke is buried at a depth of 50 m and extends to 400 m depth at a dip angle of 45°. The gray scale indicates density in g/cm^3.

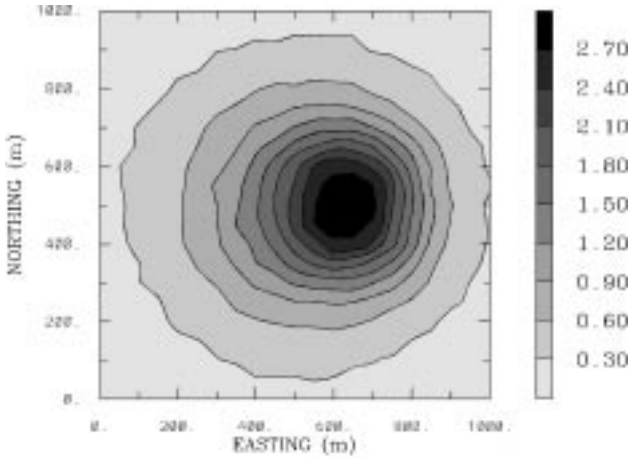

FIG. 2. The gravity anomaly produced by the dyke model in Figure 1. The data have been contaminated by uncorrelated Gaussian noise whose standard deviation is equal to 0.001 mGal plus 2% of the datum magnitude. The gray scale indicates the gravity data in mGal.

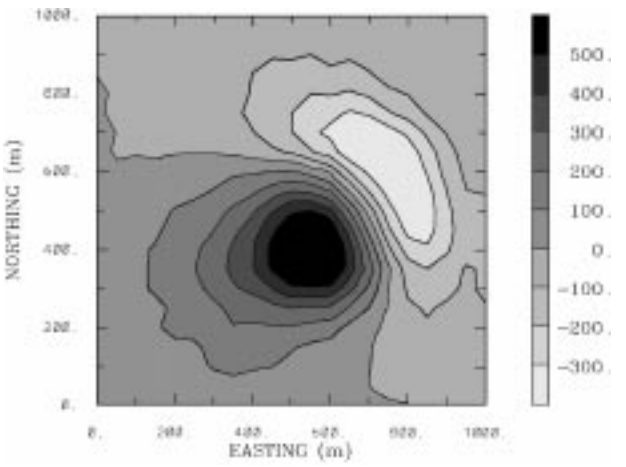

FIG. 3. The total field pseudomagnetic data calculated from the gravity data shown in Figure 2. The assumed direction of the inducing field is $I = 45°$, $D = 45°$. The gray scale indicates the magnetic anomaly in nT.

Poisson's relation and a magnetic inversion algorithm is a valid approach and can yield reasonable results. The presence of the above difficulties, on the other hand, suggests that an inversion algorithm specifically formulated for gravity data might be more desirable.

DIRECT GRAVITY INVERSION

Methodology

The vertical component of gravity field at the ith observation location $\mathbf{r}_i$ is

$$F_z(\mathbf{r}_i) = \gamma \int_V \rho(\mathbf{r}) \frac{z - z_i}{|\mathbf{r} - \mathbf{r}_i|^3}\, dv, \tag{4}$$

where $\rho(\mathbf{r})$ is the anomalous mass distribution, and γ is Newton's gravitational constant. Here we have adopted a right-handed Cartesian coordinate system with z-axis pointing vertically downward. The objective is to recover the density ρ directly from the given gravity data F_z. Let the data-misfit be given by

$$\phi_d = \left\| W_d(\mathbf{d} - \mathbf{d}^{obs}) \right\|_2^2, \tag{5}$$

where $\mathbf{d}^{obs} = (F_{z1}, \ldots, F_{zN})^T$ is the data vector, $\mathbf{d}$ is the predicted data, $W_d = \text{diag}\{1/\sigma_1, \ldots, 1/\sigma_N\}$ and σ_i is the error standard deviation associated with the ith datum. An acceptable model is one which makes ϕ_d sufficiently small.

There are generally infinitely many models that reduce the misfit to a desired value. To find a particular model, we define an objective function of the density and minimize that quantity subject to adequately fitting the data. The details of the objective function are problem dependent, but generally we require that the model is close to a reference model, ρ_0, and that the model is smooth in three spatial directions. We choose an objective function of the form,

$$\begin{aligned}
\phi_m(\rho) = {} & \alpha_s \int_V w_s \{w(z)[\rho(\mathbf{r}) - \rho_0]\}^2\, dv \\
& + \alpha_x \int_V w_x \left\{ \frac{\partial w(z)[\rho(\mathbf{r}) - \rho_0]}{\partial x} \right\}^2 dv \\
& + \alpha_y \int_V w_y \left\{ \frac{\partial w(z)[\rho(\mathbf{r}) - \rho_0]}{\partial y} \right\}^2 dv \\
& + \alpha_z \int_V w_z \left\{ \frac{\partial w(z)[\rho(\mathbf{r}) - \rho_0]}{\partial z} \right\}^2 dv,
\end{aligned} \tag{6}$$

where the functions w_s, w_x, w_y, and w_z are spatially dependent weighting functions while α_s, α_x, α_y, and α_z are coefficients that affect the relative importance of different components in the objective function. Here, $w(z)$ is a depth weighting function.

The objective function in equation (6) has the flexibility of constructing many different models. The reference model ρ_0 may be a background model of the density that is estimated from previous investigations or it could be the zero model. The reference model would generally be included in the first term, but can be removed if desired from any of the remaining terms. The relative closeness of the final model to the reference model at any location is controlled by the function w_s. The weighting functions w_x, w_y, and w_z can be designed to enhance or attenuate structures in various regions in the model domain. The reference model and four 3-D weighting functions allow additional information to be incorporated into the inversion. The additional information can be from previous knowledge about the density contrast, from other geophysical surveys, or from the interpreter's understanding about the geologic structure and its relation to density. When this extra information is incorporated, the inversion derives a model that not only fits the data, but, more importantly, has a likelihood of representing the earth.

In analogy with magnetic inversion, the kernel functions for the surface gravity data decay with depth. As a consequence, an inversion that minimizes $\|\rho - \rho_0\|^2 = \int (\rho - \rho_0)^2\, dv$ subject to fitting the data will generate a density distribution that is concentrated near the surface. To counteract the geometric decay of the kernels and to distribute density with depth, we introduce a weighting of the form $w(z) = (z + z_0)^{-\beta/2}$ into the model objective function. The values of β and z_0 are investigated in

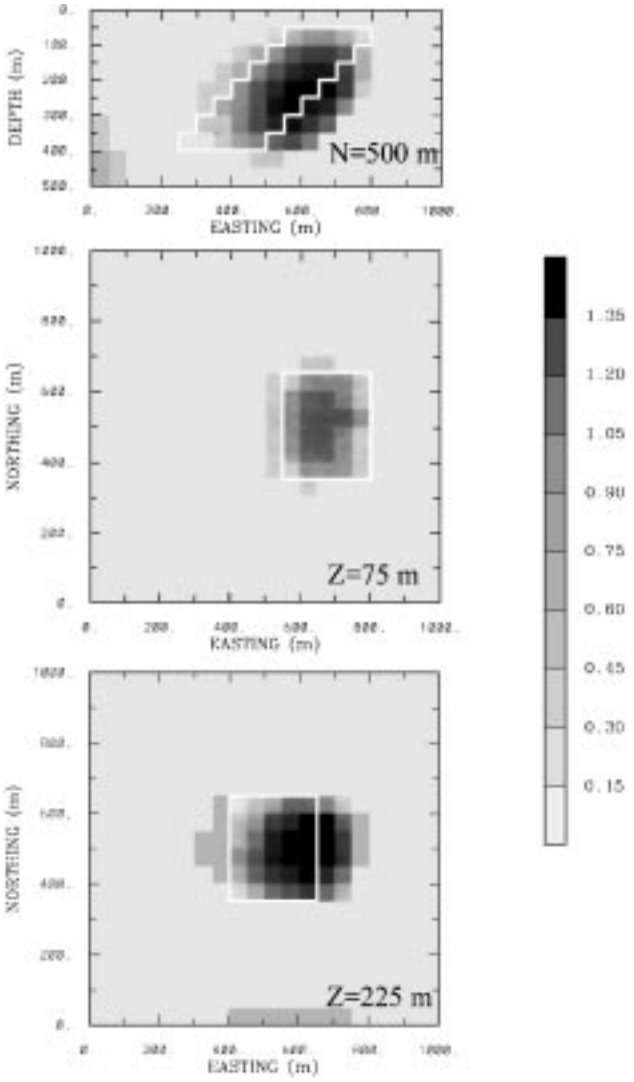

FIG. 4. The density model obtained by inverting the pseudo-magnetic data in Figure 3 using a magnetic inversion algorithm and converting the resultant susceptibility into density. The outline of the true dyke is indicated by the white lines.

the following section, but their choice essentially allows equal chance for cells at different depths to be nonzero.

To obtain a numerical solution to the inverse problem, it is necessary to discretize the problem. Let the source region be divided into cells by an orthogonal 3-D mesh and assume a constant density value within each cell. The forward modeling of gravity data defined in equation (4) then becomes the following matrix equation,

$$\mathbf{d} = \mathbf{G}\boldsymbol{\rho}, \tag{7}$$

where $\boldsymbol{\rho} = (\rho_1, \ldots, \rho_M)^T$ is the vector of cell densities. The matrix $\mathbf{G}$ has as elements G_{ij} that quantify the contribution to the ith datum of a unit density in the jth cell,

$$G_{ij} = \gamma \int_{\Delta V_j} \frac{z - z_i}{|\mathbf{r} - \mathbf{r}|^3}\, dv, \tag{8}$$

where ΔV_j is the cuboidal volume within jth cell. The closed-form solution for the integral in equation (8) has been presented in Nagy (1966), Okabe (1979), and others. The evaluation of G_{ij} is straightforward.

Using a finite-difference approximation, the model objective function defined in equation (6) can be written as,

$$\phi_m(\boldsymbol{\rho}) = \|\mathbf{W}_\rho(\boldsymbol{\rho} - \boldsymbol{\rho}_0)\|_2^2, \tag{9}$$

where $\boldsymbol{\rho}$ and $\boldsymbol{\rho}_0$ are M-length vectors. The model weighting matrix $\mathbf{W}_\rho$ incorporates the coefficients and weighting functions used to define equation (6).

The inverse problem is solved by finding a model $\boldsymbol{\rho}$ that minimizes ϕ_m and misfits the data by a predetermined amount. This is accomplished by minimizing $\phi(\boldsymbol{\rho}) = \phi_m + \lambda^{-1}(\phi_d - \phi_d^*)$, where ϕ_d^* is our target misfit and λ is a Lagrange multiplier. The minimization is carried out using a generalized subspace technique in which the solution is obtained iteratively, and only a small number of search vectors are used in each iteration to avoid the large amount of computations required to solve large matrix systems. In addition, positivity or negativity is readily incorporated into the minimization in the subspace algorithm when a nonnegative or nonpositive density model is desirable. Readers are referred to Li and Oldenburg (1996) for details of the discretization of the model objective function and the implementation of the subspace technique and positivity.

Depth weighting

Gravity data, like any static potential field data, have no inherent depth resolution. When minimizing $\|\rho\|^2 = \int \rho^2\, dv$, structures tend to concentrate near the surface regardless of the true depth of the causative bodies. This arises because the constructed model is a linear combination of kernels that decay rapidly with depth. The tendency to concentrate density at the surface can be overcome by introducing a depth weighting to counteract the natural decay of the kernels. It has been demonstrated in the magnetic inversion (Li and Oldenburg, 1996) that a weighting function that approximately compensates for the kernel's natural decay gives cells at different depths equal probability to enter into the solution with a nonzero value. Without repeating the details, we present the depth weighting appropriate for gravity inversion and illustrate it with the inversion of gravity data from a single cube at different depths.

The gravitational effect decays with the inverse distance squared. It is therefore reasonable to approximate the decay of the kernels with depth by a function of the form $(z + z_0)^{-2}$. By adjusting the value of z_0, a good match can be obtained between this function and the decay of the gravity kernels for a given mesh and observation height. It is natural to use $w(z) = (z + z_0)^{-1}$ as a weighting function but for generality, we use

$$w(z) = \frac{1}{(z + z_0)^{\beta/2}}, \tag{10}$$

where β is usually equal to 2 and z_0 depends upon the cell size of the model discretization and the observation height of the data.

We have tested the weighting function by inverting the noise-contaminated data from buried cubes. The cube is 200 m on a side and buried at a depth of 50, 100, and 150 m, respectively. The density of the cube is 1.0 g/cm^3. The model for the inversion consists of 4000 cells in a volume that is 1000 m in both horizontal directions and 500 m in depth. The model objective function includes only the first term in equation (6). The 3-D weighting function is set to unity and the depth weighting function has $z_0 = 16.8$ m, which is calculated from the given mesh by setting $\beta = 2.0$. Figure 5 shows the cross-sections through the center of the inverted density model. Superimposed on the sections are the outlines of the true cubes. Figures 5a, 5b, and 5c are the models obtained without positivity. The models are characterized by broad tails at depth, but the peaks of the recovered anomaly are at the depth consistent with the depth of the cube in the true models. Figures 5d, 5e, and 5f display the corresponding models obtained when positivity is imposed. The recovered anomalies also appear at the depth that corresponds well with the true depth of the cube. This demonstrates that the depth weighting function is effective in placing the recovered anomaly at depth of the true causative body.

The above analysis establishes the theoretical choice of the weighting function defined by the two parameters, β and z_0. In numerical applications we have observed that, given the z_0 derived in this manner, the inversions using a weighting function defined by β in the range of $1.5 < \beta \leq 2.0$ produces satisfactory results. Inversion with β slightly less than 2.0 does seem to converge more easily and, for numerical reasons, our algorithm usually sets β to a value less than 2.

Examples

As a first example, we invert the gravity data shown in Figure 2, which was produced by a single dipping dyke having a density of 1.0 g/cm^3 and shown in Figure 1. There are 441 data and 2% independent Gaussian noise has been added. To invert these data, we use a model consisting of 4000 cells of 50 m on a side. We minimize a model objective function defined in equation (6) in which $\alpha_s = 0.0005$ and $\alpha_x = \alpha_y = \alpha_z = 1.0$. All 3-D weighting functions are set to unity and the depth weighting parameters are calculated according to the procedure described in the preceding section. The inversion incorporates positivity. The recovered density model, shown in Figure 6, is a good representation of the true model in Figure 1. Both the tabular shape and the dip of the high density region are shown clearly. The recovered amplitude is slightly higher than the true value. This model can also be compared with the result in Figure 4 that is obtained by inverting the pseudomagnetic data. It is clear that the direct inversion of gravity data produces a superior model.

Next, we present a more complicated model consisting of two dykes dipping in opposite directions and having different widths and length but the same northward strike direction. This model is shown in one cross-section and one plan-section in Figure 7. The densities in the two anomalous regions are 0.8 and 1.0 g/cm^3, respectively. A total of 861 data are calculated on the surface at an interval of 50 m along east-west lines spaced 100 m apart. Figure 8 shows the data contaminated noise of 2% plus 0.05 mGal. We invert these data with, and without, a positivity constraint. When the inversion is carried out without positivity, it produces the density model shown in Figure 9. The two anomalous regions of high density and the strike direction and length of each anomaly are well defined. However, there is a broad zone of intermediate density beneath the two dykes and zones of negative density outside the main anomalies. Inverting the data in Figure 8 with the requirement that the density be positive produces the model in Figure 10. This model contains little excessive structure and no regions of negative densities. The recovered density anomalies are concentrated around the position of the true dykes, which are outlined by the white lines. The dipping structure of the longer dyke can now be readily inferred from the model.

The difference between the two inverted models in Figures 9 and 10 illustrates the effect of imposing positivity (or negativity) when it is justified by the data—it has helped produce a density distribution that is more representative of the true model. This is true in general since imposition of positivity eliminates otherwise acceptable models that have features not present in the true model, namely the negative densities, and therefore it restricts the admissible models to those that are more likely to simulate the density variations in the earth. For this reason, the positivity (or negativity) should be imposed whenever the data justify a model of positive (or negative) density contrast only.

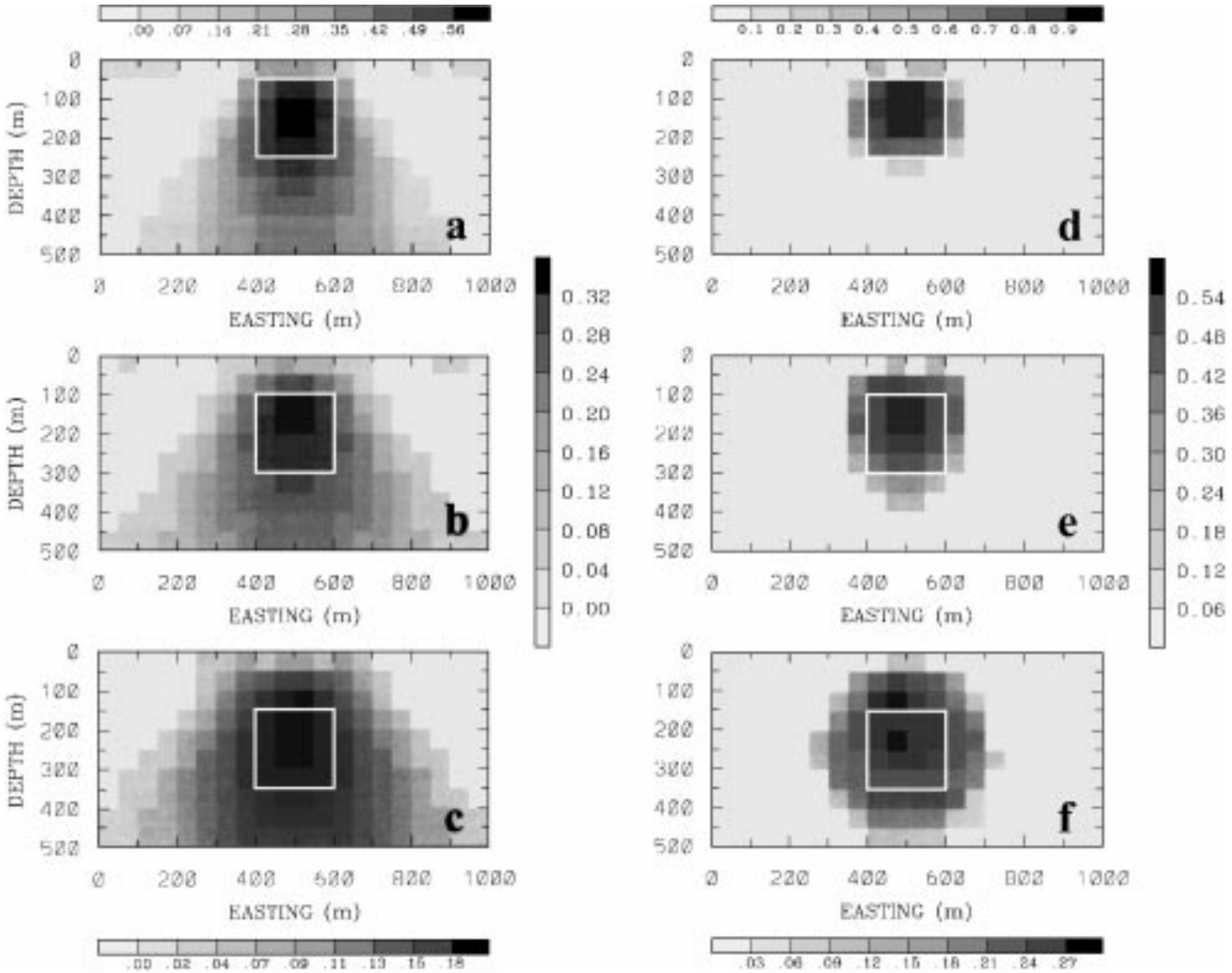

FIG. 5. Illustration of the effect of the depth weighting function. The noise-contaminated gravity data produced by a cube buried at different depths are inverted by minimizing a model objective function that incorporates the depth weighting. Cross-sections through the center of the recovered models are shown. The true position of the cube is outlined by the white box. The panels on the left are models obtained without positivity and the panels on the right are the models obtained with positivity imposed. As the true source depth increases and, as a result, the high-frequency content in the data decreases, the recovered model becomes increasingly smooth and attains a smaller amplitude. However, the depth of the recovered model is close to the true value.

FIELD APPLICATION

We now apply the inversion algorithm to field data acquired at the Stratmat Main Zone of Health Steele copper-lead-zinc deposit in northern New Brunswick. The deposit is situated in an area that is underlain by felsic to mafic and metasedimentary rocks and hosts a number of base metal sulphide deposits. The massive sulphide ore body of the Stratmat Main Zone is in a thick sequence of crystal tuffs, and dips southwest with a dip angle varying from 40° to 70°. A large meta-gabbro intrusion is adjacent to the ore body and assimilates portions of it. Gravity data were collected at a 25 m interval along north-south lines spaced 100 m apart. Figure 11 shows the Bouguer anomaly in the 1×1 km area. The elevation of the area increases from east to west and the total relief is 30 m. The Bouguer gravity data show a concentrated high at (12800E, 10400N) above the massive sulphide body. This anomaly is superimposed upon moderately high-valued anomalies associated with the gabbro intrusion. The visual inspection clearly shows the horizontal locations of the gabbro intrusion and the high density sulphide body, but inversions are needed to extract depth information and to better delineate boundaries.

There are 443 data shown in Figure 11 and we have assigned each an error of 2%. To invert these data, we use a mesh with cell widths of 50 m in easting and 25 m in northing. The thickness of the cells varies from 10 m at the surface to 40 m at the depth of 300 m. Padding cells of increasing size extend the model outward by 150 m in all horizontal directions and downward to a depth of 700 m. Drill-hole information suggests that

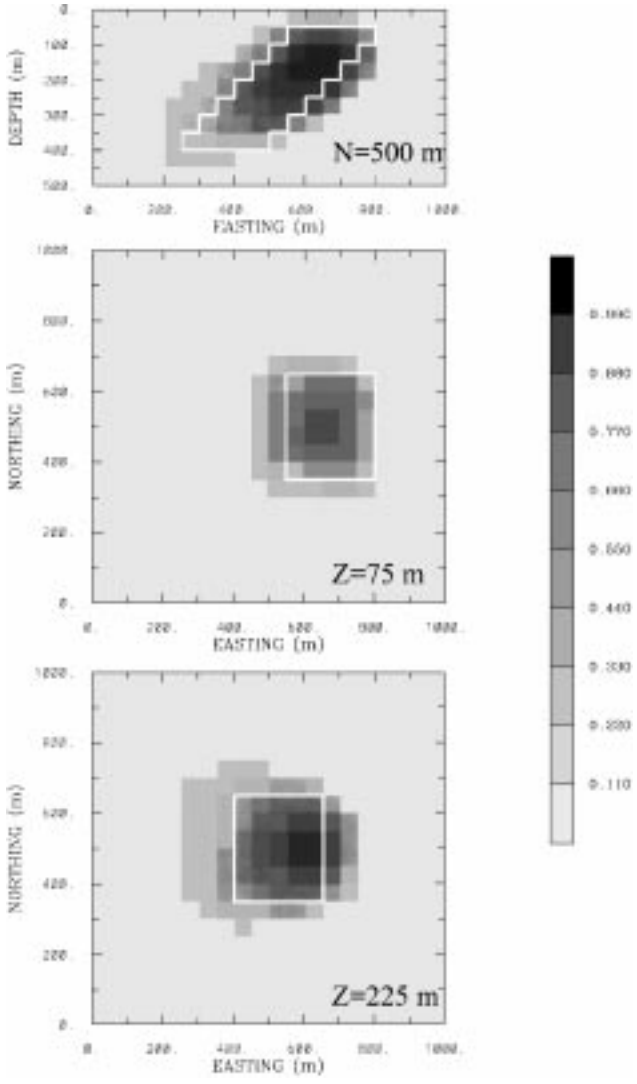

FIG. 6. The density model obtained by directly inverting the gravity data in Figure 2. The white lines indicate the outline of the true dyke with a high density contrast. The anomaly is better defined in both the spatial extent and amplitude then it is in Figure 4.

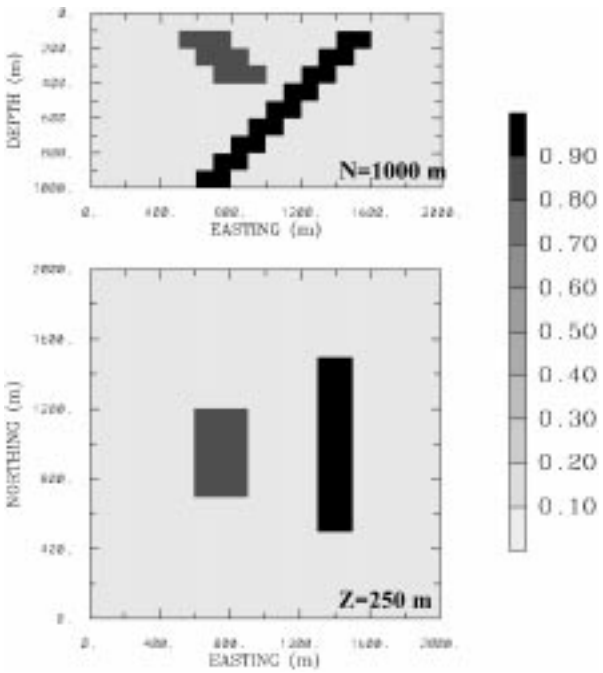

FIG. 7. The density model composed of two dipping dykes buried in a uniform background. The small dyke on the left has a density contrast of 0.8 g/cm^3 and the longer dyke on the right has a density contrast of 1.0 g/cm^3.

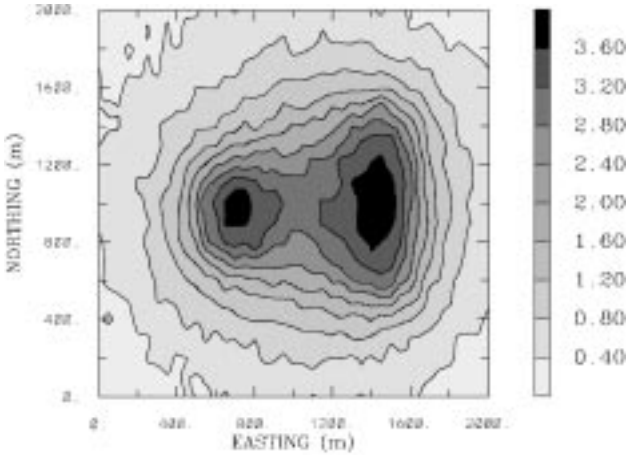

FIG. 8. The gravity anomaly produced by the density model shown in Figure 7. Each datum has been contaminated by uncorrelated Gaussian noise of 0.05 mGal and 2% of the datum magnitude.

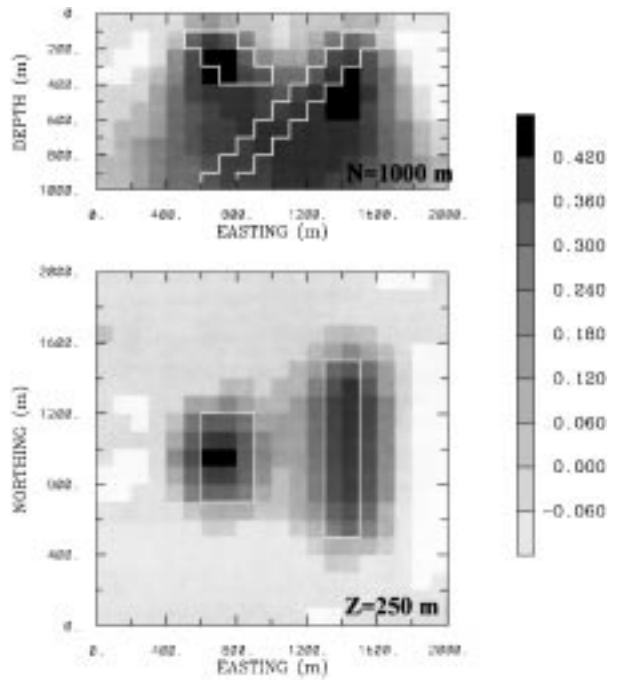

FIG. 9. The density model recovered by inverting the gravity data shown in Figure 8. The inversion has no restriction on the sign of the density contrast in the final model. The positions of the true density anomalies are indicated by the white lines. The presence of the two separate anomalies is evident, but the image is masked by the long tails and by regions of negative density.

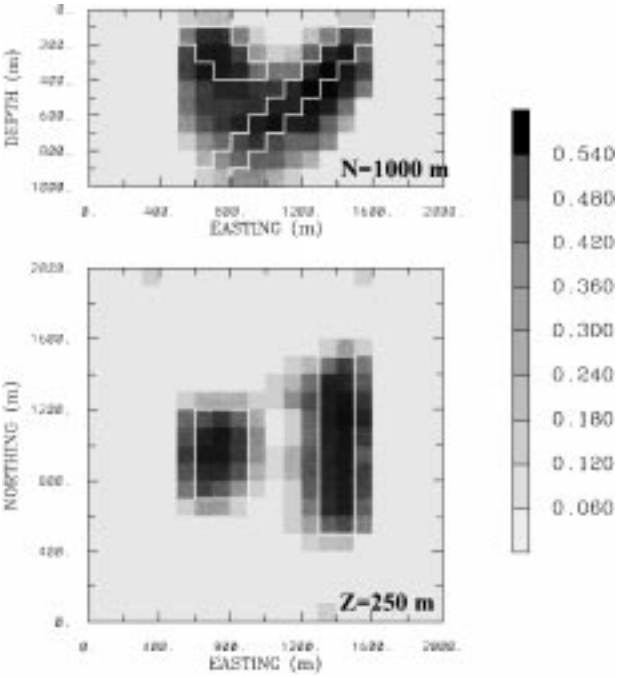

FIG. 10. The density model recovered by inverting the gravity data shown in Figure 8 with positivity imposed to produce an entirely positive density distribution. The positions of the true density anomalies are indicated by the white lines. This model provides a clearer image of the true density and the dipping structure of the longer dyke is readily inferred.

sulphide is the most dense unit in the area, followed by the gabbro intrusion that is more dense than the host. Therefore, it is reasonable to assume that the anomaly is produced by positive density contrasts and to invert for a nonnegative density model by imposing positivity. Figure 12 displays the recovered density model from the direct inversion in three cross-sections along the north-south direction. Overlaid on the sections are the outlines of the massive sulphide body. The inverted density model shows the extent of the sulphide body and its dip direction and angle. This is very encouraging given that the inversion is carried out without using any prior information about the geology.

DISCUSSION

We have developed two approaches for inverting surface gravity data to recover the causative 3-D density distributions. In the first approach, the gravity data are transformed into pseudomagnetic data using Poisson's relation, and an existing magnetic inversion algorithm is used to carry out the inversion. When measured gravity gradiometer data are available, they can be treated as pseudomagnetic data and inverted using this approach. Any component of the gradiometer data can be inverted individually or multiple components can be inverted jointly. In the second approach, the gravity data are inverted directly by minimizing an objective function of the density model subject to fitting the observations. The model objective function has the ability to incorporate prior information into the inversion via a reference model and 3-D weighting functions. A crucial feature of the objective function is a depth weighting function that counteracts the natural decay of the kernel functions. The parameters of this depth weighting depend on the discretization of the model but they are calculated easily. When the gravity data are known to be produced by positive density contrasts, this can be incorporated into the inversion and it has been shown to improve the solution. Applications of our methods to synthetic data sets have produced density models

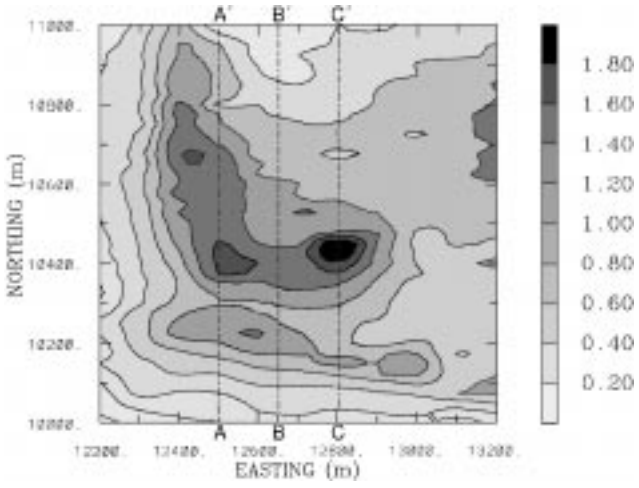

FIG. 11. Gravity anomaly data consisting of 443 observations from the Heath Steele Stratmat copper-lead-zinc deposit in northern New Brunswick. The peak at (12800E, 10400N) is produced by a massive sulphide orebody and it is superimposed on linear anomalies produced by gabbroic intrusions. The dashed lines are the positions at which cross-sections of the inverted density model will be shown.

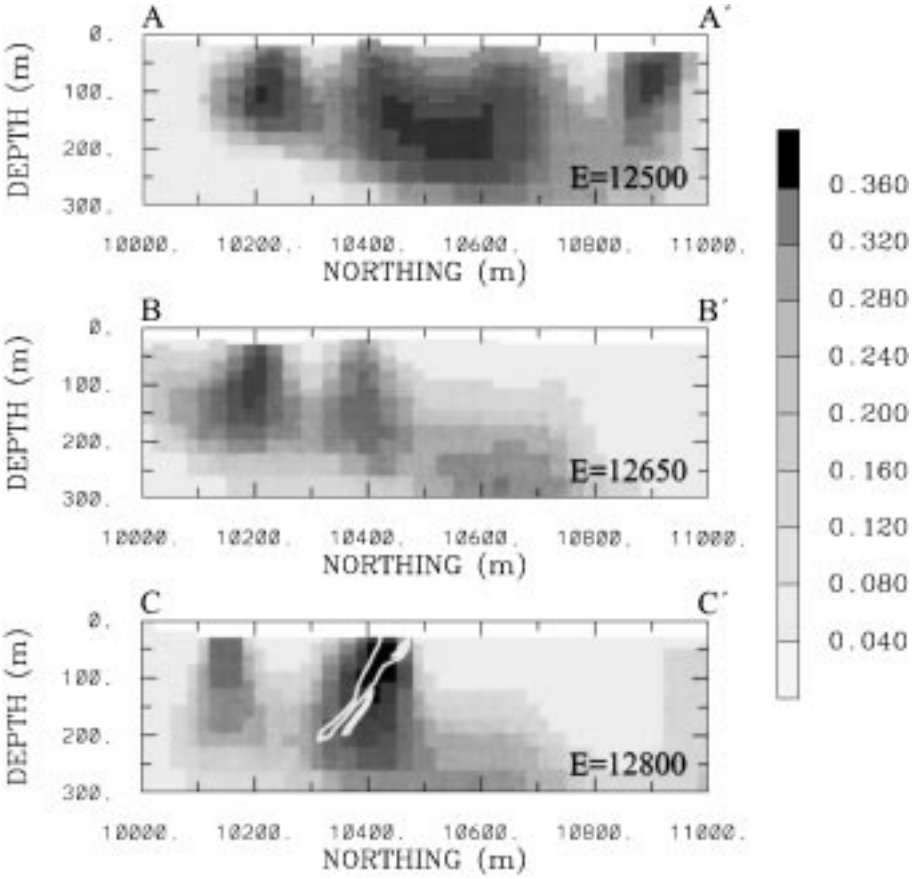

FIG. 12. The density model obtained by inverting the field gravity data shown in Figure 11. The positions of these three sections are indicated in the data map. Positivity has been imposed during the inversion. The white lines in the section 12800E indicate the outline of the massive sulphide body obtained through drill hole information.

representative of the true structures, and the inversion of field data has produced a density model consistent with the geology.

ACKNOWLEDGMENTS

This work was supported by an NSERC IOR grant and an industry consortium "Joint and Cooperative Inversion of Geophysical and Geological Data." Participating companies are Placer Dome, BHP Minerals, Noranda Exploration, Cominco Exploration, Falconbridge, INCO Exploration & Technical Services, Hudson Bay Exploration and Development, Kennecott Exploration Company, Newmont Gold Company, Western Mining Corporation, and CRA Exploration Pty.

REFERENCES

Baranov, V., 1957, A new method for interpretation of aeromagnetic maps: Pseudogravimetric anomalies: Geophysics, **22**, 359–383.
Bhattacharyya, B. K., 1965, Two-dimensional harmonic analysis as a tool for magnetic interpretation: Geophysics, **30**, 829–857.
Chai, Y., and Hinze, W. J., 1988, Gravity inversion of an interface above which the density contrast varies exponentially with depth: Geophysics, **53**, 837–845.
Clarke, G. K. C., 1969, Optimum second-derivative and downward continuation filters: Geophysics, **34**, 424–437.
Grant, F. S., and West, G. F., 1965, Interpretation theory in applied geophysics, McGraw-Hill Book Co.
Green, W. R., 1975, Inversion of gravity profiles by use of a Backus-Gilbert approach: Geophysics, **40**, 763–772.
Guillen, A., and Menichetti, V, 1984, Gravity and magnetic inversion with minimization of a specific functional: Geophysics, **49**, 1354–1360.
Guspi, F., 1992, Three-dimensional Fourier gravity inversion with arbitrary density contrast: Geophysics, **57**, 131–135.
Hinze, W. J., 1990, The role of gravity and magnetic methods in engineering and environmental studies, *in* Ward, S. H., Ed., Geotechnical and environmental geophysics, Vol. 1, Soc. Expl. Geophys., 75–126.
Last, B. J., and Kubik, K, 1983, Compact gravity inversion: Geophysics, **48**, 713–721.
Li, Y., and Oldenburg, D. W., 1996, 3-D inversion of magnetic data: Geophysics, **61**, 394–408.
Nagy, D., 1966, The gravitational attraction of a right rectangular prism: Geophysics, **31**, 361–371.
Okabe, M., 1979, Analytical expressions for gravity anomalies due to homogeneous polyhedral bodies and translations into magnetic anomalies: Geophysics, **44**, 730–741.
Oldenburg, D. W., 1974, The inversion and interpretation of gravity anomalies: Geophysics, **39**, 394–408.
Paterson, N. R., and Reeves, C. V., 1985, Applications of gravity and magnetic surveys: The state-of-the-art in 1985: Geophysics, **50**, 2558–2594.
Pedersen, L. B., 1977, Interpretation of potential field data: A generalized inverse approach: Geophys. Prosp., **25**, 199–230.
———1979, Constrained inversion of potential field data: Geophys. Prosp., **27**, 726–748.
Reamer, S. K., and Ferguson, J. F., 1989, Regularized two-dimensional Fourier gravity inversion method with application to the Silent Canyon Caldera, Nevada: Geophysics, **54**, 486–496.
Ward, S. H., Ed., 1990, Geotechnical and environmental geophysics, Soc. Expl. Geophys.
Wiener, N., 1949, Extrapolation, interpolation, and smoothing of stationary time series: Cambridge, MIT Press.

APPENDIX

CALCULATION OF PSEUDOMAGNETIC DATA

Given a causative body with magnetic susceptibility κ and density ρ, if the susceptibility and density have a constant ratio κ/ρ, the Poisson's relation (e.g., Baranov, 1957; Grant and West, 1965) states that the magnetic field **B** and gravity field **F** are related by

$$\mathbf{B}(\mathbf{r}) = \frac{B_0\kappa}{4\pi\gamma\rho}\frac{\partial}{\partial\hat{u}}\mathbf{F}(\mathbf{r}), \tag{A-1}$$

where $\partial/\partial\hat{u}$ denotes the directional derivative. B_0 is the strength of the inducing magnetic field that is in the direction of $\hat{u}$, and γ is the gravitational constant. The component of magnetic anomaly in the direction $\hat{v}$ is given by

$$B_v(\mathbf{r}) = \frac{B_0\kappa}{4\pi\gamma\rho}\hat{v}\cdot\frac{\partial}{\partial\hat{u}}\mathbf{F}(\mathbf{r}), \tag{A-2}$$

Expressing the gravitational field as $\mathbf{F}(\mathbf{r}) = -\nabla U(\mathbf{r})$, were $U(\mathbf{r})$ is the gravitational potential, we can rewrite equation (A-2) as

$$B_v(\mathbf{r}) = -\frac{B_0\kappa}{4\pi\gamma\rho}\frac{\partial}{\partial\hat{v}}\frac{\partial}{\partial\hat{u}}U(\mathbf{r}). \tag{A-3}$$

Thus if the gravitational potential is known, the magnetic anomaly in any direction can be calculated for an arbitrary inducing field $\mathbf{B}_0$.

The gravimetric data collected in a geophysical survey gives the distribution of vertical component of the earth's gravitational field over an area,

$$F_z(x,y) = -\frac{\partial}{\partial z}U(x,y,z)\bigg|_{z=0}, \tag{A-4}$$

where the coordinate system has z-axis pointing down vertically, and the observation plane is assumed to be $z=0$. Let $\tilde{f}(p,q) = \mathcal{F}_{xy}[f(x,y)]$ denote the 2-D Fourier transform of $f(x,y)$, where (p,q) are transform variables in x- and y-direction. Since we have, from the classic potential field theory, that

$$\mathcal{F}_{xy}\left[\frac{\partial}{\partial z}U(x,y,z)\right] = \sqrt{p^2+q^2}\,\mathcal{F}_{xy}[U(x,y,z)], \tag{A-5}$$

the gravitational potential is given by

$$\tilde{U}(p,q) = -\frac{1}{\sqrt{p^2+q^2}}\tilde{F}_z(p,q). \tag{A-6}$$

on the observation plane. At any height above the plane it is given by

$$\tilde{U}(p,q) = -\frac{1}{\sqrt{p^2+q^2}}\tilde{F}_z(p,q)e^{z\sqrt{p^2+q^2}}. \tag{A-7}$$

Using the identity that the directional derivative in the spatial domain is expressed in the wavenumber domain by the multiplication of the inner product of the directional vector and the wavenumber vector, we obtain,

$$\mathcal{F}_{xy}\left[\frac{\partial}{\partial\hat{u}}f(x,y,z)\right] = (\hat{u}\cdot\mathbf{K})\mathcal{F}_{xy}[f(x,y,z)], \tag{A-8}$$

where $\mathbf{K} = (ip, iq, \sqrt{p^2+q^2})$ is the wavenumber vector and $i=\sqrt{-1}$. We can take the 2-D Fourier transform of equation (A-3) and substitute into equation (A-6) to obtain the Fourier transform of the magnetic anomaly on the observation plane ($z=0$) as,

$$\tilde{B}_v(p,q) = \frac{B_0\kappa}{4\pi\gamma\rho}\frac{(\hat{u}\cdot\mathbf{K})(\hat{v}\cdot\mathbf{K})}{\sqrt{p^2+q^2}}\tilde{F}_z(p,q). \tag{A-9}$$

Equation (A-9) thus relates the 2-D Fourier transform of the magnetic anomaly to that of gravity data due to the same causative body with a constant ratio $\lambda=\kappa/\rho$. Given a set of gravity data, this equation can be used to generate the corresponding pseudomagnetic data when the ratio κ/ρ, the parameters of the inducing magnetic field, and the direction of anomaly projection are assumed. The term pseudomagnetic is used to denote the magnetic field that is calculated from the gravity data via equation (A-9) and is not related to real distribution of magnetic sources.

The operator in equation (A-9) is stable and the calculation of the pseudomagnetic data can be carried out easily using fast Fourier transform (FFT) when gridded gravity data are available. However, since the operator is essentially a first-order differential, it will amplify the noise components with increasing wavenumber. A low-pass filter is therefore necessary to suppress the effect of noise in the field data. The pseudomagnetic data are calculated from the smoothed gravity data. We effect the smoothing by Wiener filtering (Wiener, 1949),

$$h(p,q) = \frac{P_t - P_n}{P_t}, \tag{A-10}$$

where P_t and P_n are the power spectra of the observed gravity data (including contaminating noise) and the noise, respectively. Clarke (1969) used this to suppress noise in the second-derivative and downward-continuation operation of potential-field data.

The power spectrum of the data, P_t, is calculated from the Fourier transform of gravity data directly, but the noise power spectrum P_n needs to be estimated. Since the gravity data are to be inverted, each datum has an associated estimate of error standard deviation. It is usually different for each datum. Assuming the contaminating noise is a Gaussian random variable with zero mean and is uncorrelated, the power spectrum of the noise contaminating the entire data set is flat and P_n is a constant. For each assumed value of P_n the filter in equation (A-10) can be applied to the gravity data to produce smoothed data and the χ^2 misfit between the observed and smoothed data can be computed. The final estimated value P_n^{est} is that which gives χ^2 its expected value, the number of observed gravity data. This is the optimum amount of smoothing that can be applied to the data for the purpose of noise suppression. Figure A-1 summarizes the processing as applied to the gravity data shown in Figure 2. Figure A-1a displays the χ^2 misfit as a function of the assumed noise power spectrum. The dashed line indicates the expected value of the misfit. The abscissa of the intersection between the dash line and the curve yields the P_n^{est} for this data set. Figure A-1b is the radially averaged power spectrum of the gravity data with the P_n^{est} being indicated by the dashed line. Figure A-2 displays the comparison between the pseudomagnetic field calculated using the above procedure and that calculated analytically. They agree well.

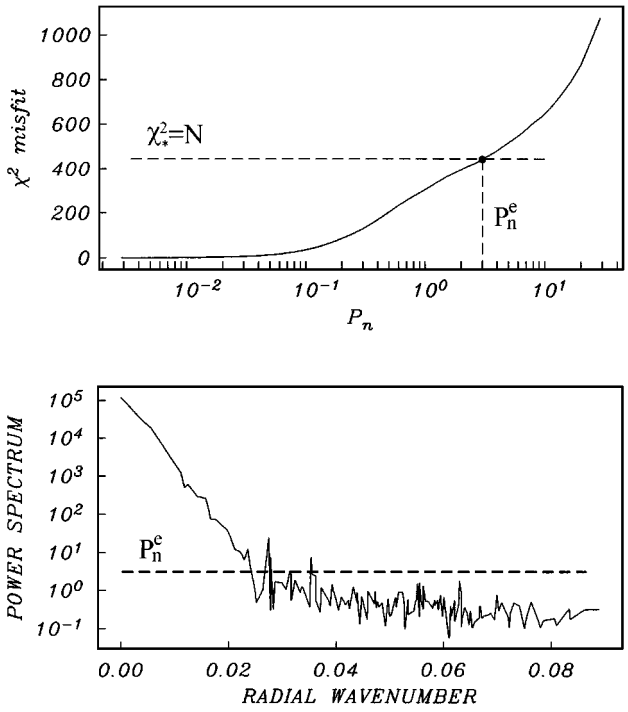

FIG. A-1. The amount of smoothing applied to the gravity data before being transformed to the pseudomagnetic data is chosen such that the χ^2 misfit between the original and smoothed gravity data is equal to the number of data. The upper panel shows the misfit as a function of the assumed noise power spectrum. The dashed line gives the expected χ^2 misfit of 441 and its intersection with the solid line determines the estimated power of the noise. The lower panel shows the radially averaged power spectrum of the gravity data. The dashed line shows the estimated noise power spectrum obtained from the upper panel.

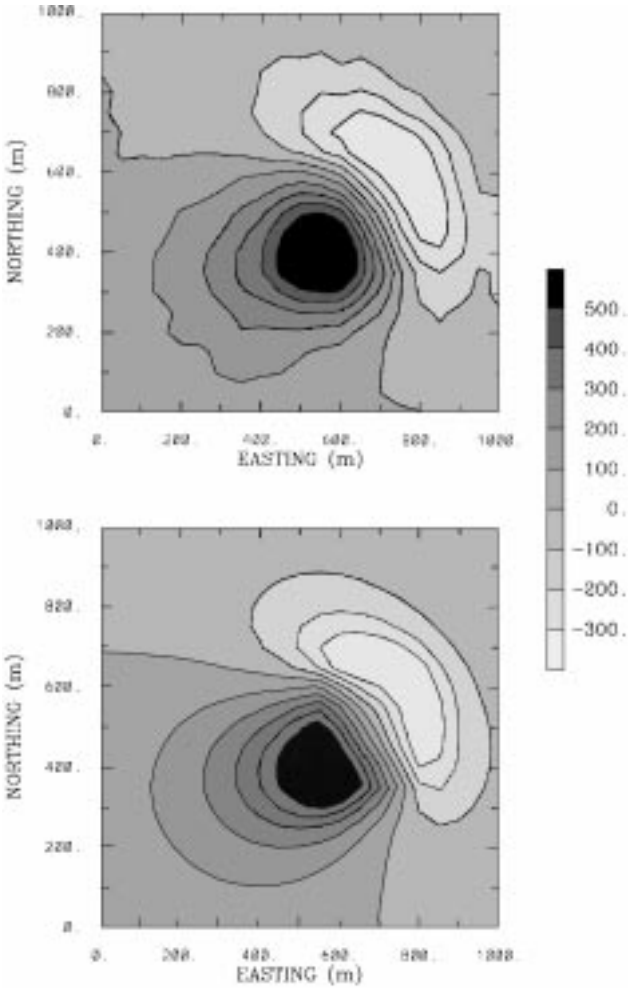

FIG. A-2. Comparison between the numerically and analytically calculated pseudomagnetic data. The upper panel is the total field pseudomagnetic anomaly obtained through the numerical transformation from the noise-contaminated gravity data in Figure 2. The inducing field has direction $I = 45°$, $D = 45°$. The lower panel shows the same anomaly calculated directly through a magnetic forward modeling from the model shown in Figure 1. Note the two maps agree well, with the most obvious discrepancy being the effect of the noise in the numerical results.